Journal of Materials Science: Materials in Electronics
https://doi.org/10.1007/s10854-019-01039-z

# Physical properties evaluation of nebulized spray pyrolysis prepared Nd doped ZnO thin films for opto-electronic applications

A. Rohini Devi[1] · A. Jegatha Christy[1] · K. Deva Arun Kumar[2] · S. Valanarasu[2] · Mohamed S. Hamdy[3] · K. S. Al-Namshah[3] · Abdullah M. Alhanash[3] · Dhanasekaran Vikraman[4] · Hyun-Seok Kim[4]

Received: 22 November 2018 / Accepted: 28 February 2019


**Abstract**
Thin films of neodymium (Nd) doped zinc oxide (NZO) were coated onto glass substrates at 400 °C by nebulized spray pyrolysis using different doping weight percentage (wt%) of Nd. The prepared films were exhibited in hexagonal structure of polycrystalline nature along with (002) preferential orientation. Morphological properties and elemental compositions were performed by scanning electron microscopy and energy dispersive by X-ray, respectively. Tauc's plot discovered the optical energy band gap of 3.17 eV for 5 wt% Nd doped NZO film. PL profiles depicted a solid green emission peak at around 680 nm at room temperature. Optical constants such as refractive indices, dielectric constants, carrier concentration and plasma frequency were evaluated for NZO through optical approximation route. Hall mobility and carrier concentrations were enhanced with rise of Nd doping wt%. A drastic change in the resistivity was observed due to incorporation of Nd dopant and it has evidently demonstrated in detail.

## 1 Introduction

In the recent decades, transparent conducting oxides (TCO) such as tin dioxide cadmium oxide and zinc oxide are highly attracted materials because of their potentials for various uses. Among them, zinc oxide (ZnO) is a hopeful TCO material due to their flared feasibility to use as gas sensing, photo-electrochemical, catalytic, piezoelectric, and optoelectronic applications [1]. ZnO is a group of II–VI functional semiconductor material and has a noteworthy attention because of its eco-friendly behavior, large exciton binding energy, wide band gap and high chemical stability [2, 3]. Recently, nanostructures of ZnO with dopant elements were used to perceive the better optical and electrical behaviors [4–6]. The various fabrication routes were used to coat undoped and doped ZnO films by RF sputtering [7], successive ionic layer adsorption and reaction (SILAR) [6, 8], thermal evaporation [9], sol–gel [10], spray pyrolysis technique [11], and chemical vapor deposition (CVD) [12]. In earlier, the different metals such as aluminum, indium and gallium doped ZnO were investigated plausibly [13–15].

In recent times, ZnO doped with rare earth metals (Pr, Eu, Nd, Sm, Gd, and Yi) are an fascinating materials owing to their capability by doping metal to alter the electrical and optical properties as a potential candidate for optoelectronic applications [16, 17]. Theoretical simulations was revealed the n-type behavior of neodymium (Nd) doped ZnO (NZO) due to its donor state observation nearer with the conduction band [18, 19]. Also, NZO film can be achieved the good electrical conductivity by downshifting/conversion layers within the host lattice structure through the Nd doping [20]. Also, the NZO films are very promising for the photo induced Pockels effects which is extended the interest of this work [20]. Liu et al. [21] revealed from the deep investigation of NZO electrical and optical properties that $Nd^{3+}$ ions played asa carrier donors and the energy transfer from host to $Nd^{3+}$ significantly improved to use as an efficient material for optoelectronic devices.

✉ Dhanasekaran Vikraman
v.j.dhanasekaran@gmail.com

✉ Hyun-Seok Kim
hyunseokk@dongguk.edu

[1] Department of Physics, Jayaraj Annapackiam College for Women, Periyakulam, Theni 625601, India

[2] PG and Research Department of Physics, Arul Anandar College, Karumathur, Madurai 625514, India

[3] Chemistry Department, College of Science, King Khalid University, P.O. Box 9004, Abha 61413, Saudi Arabia

[4] Division of Electronics and Electrical Engineering, Dongguk University-Seoul, Seoul 04620, Republic of Korea

Published online: 07 March 2019

NZO films were successfully coated by different routes including spray pyrolysis [22], sol–gel [23], pulsed-laser deposition [24], and pulsed electron beam deposition [25]. Among them, the spray pyrolysis method offers a low-cost and large area growth of NZO thin films. Furthermore, the deposition of film is simply adjusted by the coating parameters such as substrate to nozzle distance, spray rate, substrate temperature and dopant concentration. In the present work, thin films of rare earth metal doped NZO were coated by nebulized spray pyrolysis method on glass substrates. The doping element weight percentage (wt%) role of NZO thin films on the electrical and structural properties are deeply examined. Compared with available literatures, the detailed investigation provided based on optical properties and their constants in terms of doping concentration for NZO thin films. Moreover, for the first time to the best of our knowledge, a simplified spray technique using nebulizer is employed for the fabrication of NZO films for optoelectronic devices.

## 2 Experimental procedure

Nebulized spray pyrolysis method was employed to deposit the thin films of NZO on glass substrates as illustrated in the Fig. 1. Firstly, (0.1 M) zinc acetate dehydrate [Zn $(CH_3COO)_2{\cdot}2H_2O$] was dissolved in de-ionized water and methanol (1:3 ratio). For the doping of Nd, neodymium acetate hexahydrate [Nd $(CH_3COO)_2{\cdot}6H_2O$] was mixed with the above solution mixture using weight percentage (wt%) of 1, 3 and 5. Then, the solution mixtures were subjected to constant stirring for 15 min at room temperature to produce a homogeneous and clear solution and it was used as a source for nebulized spray technique. A 10 ml solution was used in the solution container of nebulizer unit to spray. The compressed air was allowed to pass through the nebulizer unit with the constant pressure of 1.5 Kg/cm$^2$. The ultrasonically cleansed glass substrates were placed on the hot plate and substrate temperature was maintained at 400 °C using temperature controller. The mist of precursor solution sprayed through nozzle of the gun on the substrate. The space between the spray nozzle and substrate was maintained as 50 mm. Then the deposited film was endorsed to cool gradually to room temperature.

Mitutoyo SJ-301 stylus profilometer used to validate the film thickness of NZO thin films. SEIFERT-FPM XRD7 diffractometer was employed to perform the structural analysis using Cu-$K_\alpha$ radiation. Nova Nano SEM microscope was used to analyze the morphology of NZO films. The elemental composition of NZO thin films were observed by energy dispersive analysis by X-ray (EDAX). UV–Vis–NIR spectra were recorded using Varian Cary 100 scan spectrometer. Photoluminescence (PL) spectra were observed using a He-Cd laser (325 nm) source with the excitation wavelength of 325 nm at room temperature. Carrier concentration, resistivity and mobility were estimated at room temperature with the support of ECOPIA Hall effect system.

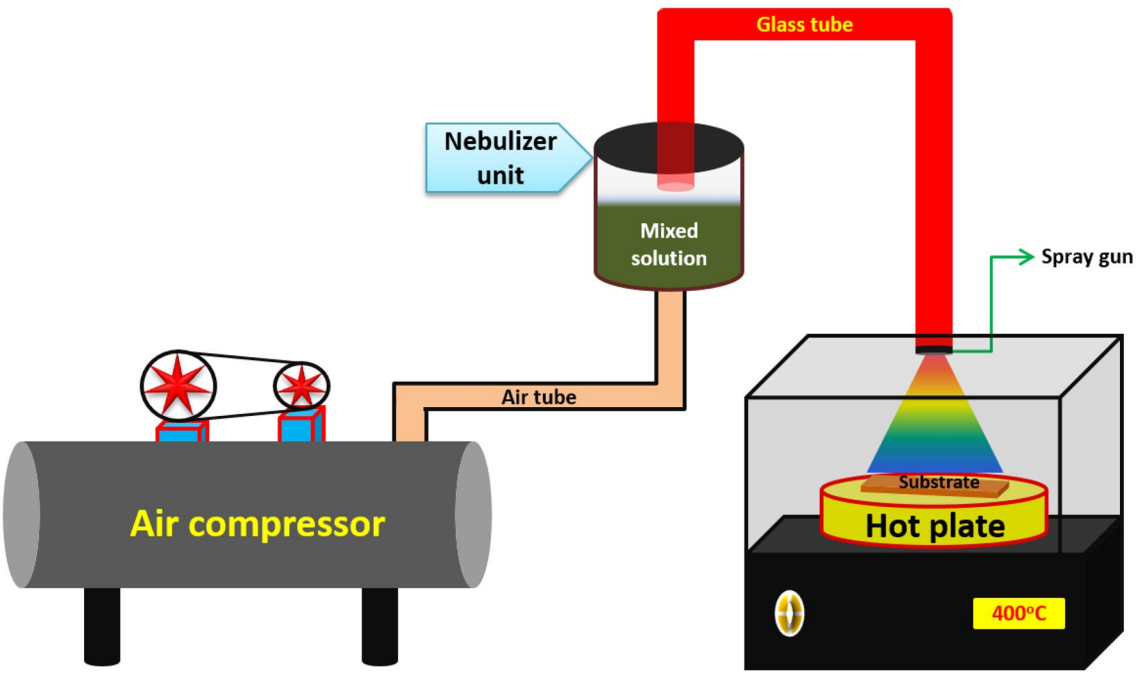


**Fig. 1** Schematic diagram of nebulized spray pyrolysis technique

## 3 Results and discussions

The different Nd doping weight percentage (wt%), such as 1, 3 and 5%, using prepared NZO thin films were coated by nebulized spray pyrolysis method on glass substrates. Figure 2a displays X-ray diffraction (XRD) patterns of 1, 3 and 5 wt% of Nd using prepared NZO films. For all the wt% using prepared NZO films, XRD diffraction patterns are observed (100), (002), (101), (102) and (103) lattice orientations. The perceived peaks are confirmed the polycrystalline nature with wurtzite structure. The predominant peak is exposed at (002) lattice plane for all the NZO films. It is obvious that all the films are composed of ZnO wurtzite phase and are in agreement with JCPDS standard data (79-2205). Also, no other new phases or impurities based peaks are observed which represented the eventually incorporation of Nd atoms in to ZnO matrix. The crystallite size was estimated using the full width at half maximum (FWHM) values of predominant (002) plane with the support of Debye Scherer relation [6, 26]. The crystallite size is reduced with the doping wt% which corresponds to increase of FWHM value. The alteration of crystallite size and FWHM with respect to doping percentage is shown in Fig. 2b, c, respectively. The calculated crystallite size is reduced from 48 to 39 nm for 1 to 5 wt% of Nd doping concentration, respectively. This variation is good agreement with previous reported result by Zheng et al. [27]. FWHM value is linearly decreased with increase of Nd doping wt%. This variation is occurred due to the ZnO internal structure modulation by Nd incorporation which stimulates the reduction of crystallite size.

Thickness is the crucial thin film factor to control the micro structural properties. The thickness (t) of the NZO is calculated using the weight gain method. The following relation is used to estimate the thickness of NZO films [28],

$$t = \frac{m}{A\rho} \tag{1}$$

where 't' is the thickness of the film, 'ρ' is the density of the film; 'A' is the area of coated film and 'm' is the weight. The calculated thicknesses are at 192, 246 and 275 nm for NZO films which prepared using at 1, 3 and 5 wt% of Nd doping, respectively. Moreover, the thickness results were validated using stylus-profilometer. The estimated thickness values were at 183, 252 and 286 nm for 1, 3 and 5 wt% of Nd doped NZO thin films, respectively. The calculated thickness values are consisted with weight-gain method observed results. The reduction of crystallite size with enhancement of film thickness is due to quantum confinement effect. Texture

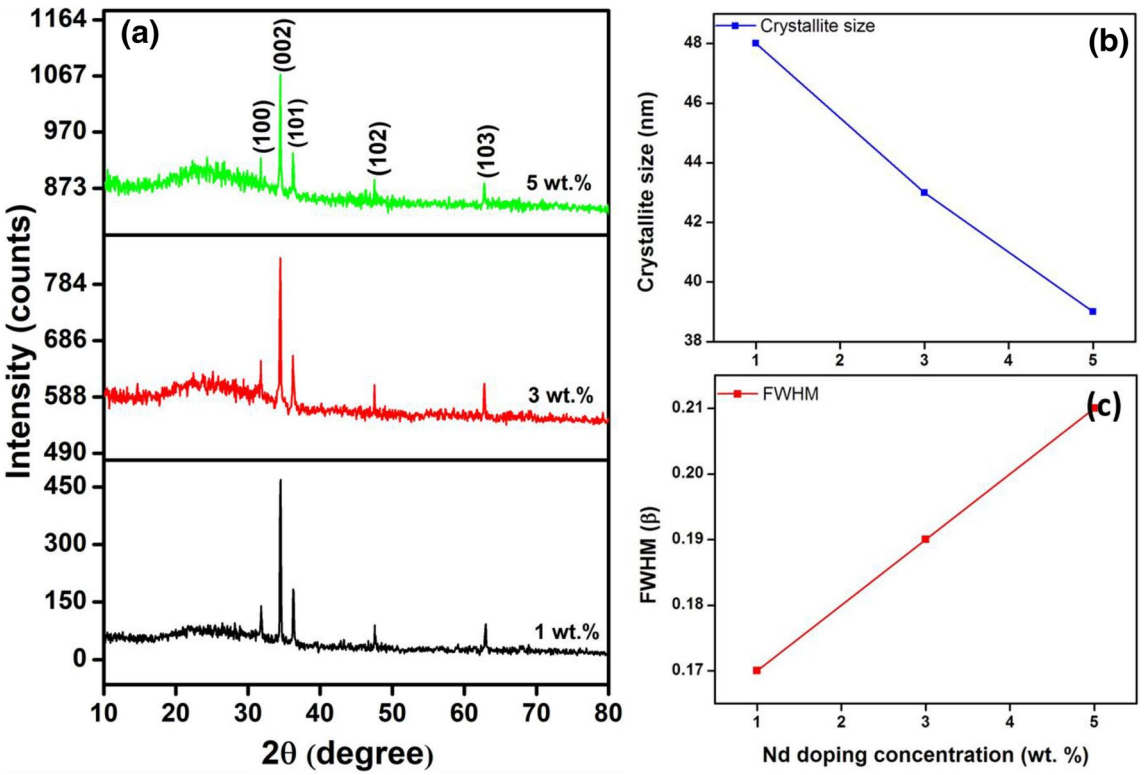


**Fig. 2** **a** XRD patterns of different Nd wt% using prepared NZO thin films; **b, c** the variations of **b** crystallite size and **c** FWHM variation for NZO thin films

coefficient TC (hkl) was derived for the preferred orientation using the relation (2) [29],

$$TC\,(hkl) = \frac{I\,(hkl)/I_0(hkl)}{N_r^{-1}\ \sum I\,(hkl)/I_0(hkl)} \tag{2}$$

where N is the reflection number, $I_{0(hkl)}$ is the standard intensity and $I_{(hkl)}$ is the measured intensity. The lattice constants of 'a' and 'c' were estimated for NZO thin films using the following Eq. (3),

$$\frac{1}{d^2} = \frac{4}{3}\left\{\frac{h^2+hk+k^2}{a^2}\right\} + \left\{\frac{l^2}{c^2}\right\} \tag{3}$$

The micro strain and dislocation density were calculated for NZO thin films as described in the earlier report [30, 31]. The assessed values of lattice constants, micro strain, dislocation density, and texture coefficient for NZO thin films are tabulated in Table 1. The micro strain and dislocation density values are observed in the range of $2.2–2.6\times10^{-3}$ and $4.53–6.32\times10^{15}$ lines/m$^2$ for 1–5 wt% of Nd doped NZO thin films, respectively. From the observed results, lattice imperfection is increased with doping wt% due to the higher ionic radius of $Nd^{3+}$ (0.99 Å) than $Zn^{2+}$ (0.60 Å). The extracted results of texture coefficient (TC) values are provided in Table 1. The increment of Nd content in the NZO film is resulting to decrease TC value for (002) plane. The lattice constants of 'a' and 'c' are slightly enhanced with Nd wt% as given in Table 1.

Furthermore, to derive the linear relation between crystallite size and strian values, 'Williamson–Hall' (W–H) analysis was used [32].

$$\Delta(2\theta)\ cos\theta = \frac{\lambda}{D} + 4\varepsilon\ sin\theta \tag{4}$$

where Δ(2θ) is peak different. Figure 3a shows the plot of Δ(2θ) cos$\theta$ versus sin$\theta$. The crystallite size and micro strain values are to be extracted by the intersection of y axis and slope, respectively using Fig. 3a. The estimated crystallite sizes by W–H method are exhibited at 45.7, 42.8 and 38.2 nm for 1, 3 and 5 wt% of Nd using prepared NZO, respectively (Fig. 3b). The observed values are consisted with the conventional route derived results as presented in Table 1. Similarly, the micro strain values are also slightly varied as given in Fig. 3c compared with its experimental values (Table 1). The observed relation clearly depicts the nano-sized crystallites in the nebulized spray pyrolysis prepared NZO films.

Scanning electron microscopy (SEM) images were used to investigate the morphology of NZO thin films. Figure 4a–c shows the SEM images of NZO thin films which prepared using 1, 3 and 5 wt%, respectively. It is clearly seen that the films having mixed shape of spherical and agglomerated cone like particles on the film surface. From the Fig. 4a, NZO film surface is clearly visualized with a smooth and homogeneous morphology which prepared using 1 wt% Nd. The agglomerated grains are observed with inhomogeneous nature for 3 and 5 wt% using prepared NZO thin films as shown in Fig. 4b, c. From the comparison of SEM micrographs, the lower doping concentration (1 wt%) is yielded a spherically shaped uniform grains without any hillocks for NZO thin film. This may be due to low lattice imperfection at 1 wt% Nd doping which is consistent with our microstructure results. The composition variations of different wt% doped NZO thin films are shown in Fig. 5a. From the EDAX profiles, Nd composition is enhanced with increase of doping wt% whereas Zn and O ions composition is linearly decreased with increase of doping wt%. Figure 5b showed the EDAX spectrum of NZO thin film which prepared using 5 wt% Nd. It is found that Zn, O and Nd are exhibited at 42.3%, 53.1% and 4.6%, respectively in NZO thin film. The EDAX result is demonstrated that the Nd ions are successfully incorporated with ZnO matrix.

PL spectroscopy is an inevitable route to analyze the luminescence behavior of NZO thin film which depends on the chemical structure, crystallite size and morphology [33]. Figure 5c describes the room temperature observed PL spectra of NZO thin films with an excitation wavelength of 325 nm. A robust emission peak is perceived at around 686 nm in PL spectra for NZO thin films. The observed emission band is due to the recombination of hole and electron from the valance band and conduction band. The observation of green emission behavior in Nd doped ZnO lattice can be associated to present of Nd atoms in the

**Table 1** Structural and optical parameters of NZO thin films

| Nd doping (wt%) | Structural parameters | | | | | Optical parameters | | |
|---|---|---|---|---|---|---|---|---|
| | Lattice constants (Å) | | Dislocation density ($\times10^{16}$) lines/m$^{-2}$ | Strain ($\times10^{-3}$) | Texture coefficient ($T_C$) | Static dielectric constant ($\varepsilon_\infty$) | Plasma frequency ($10^{15}$) s$^{-1}$ | Carrier concentration ($10^{19}$) cm$^{-3}$ |
| | *a* | *c* | | | | | | |
| 1 | 3.247 | 5.198 | 4.53 | 2.2 | 3.14 | 7.1 | 1.63 | 0.822 |
| 3 | 3.251 | 5.201 | 5.17 | 2.6 | 2.88 | 12.1 | 1.83 | 1.77 |
| 5 | 3.253 | 5.206 | 6.32 | 2.9 | 2.67 | 17.6 | 1.88 | 2.71 |

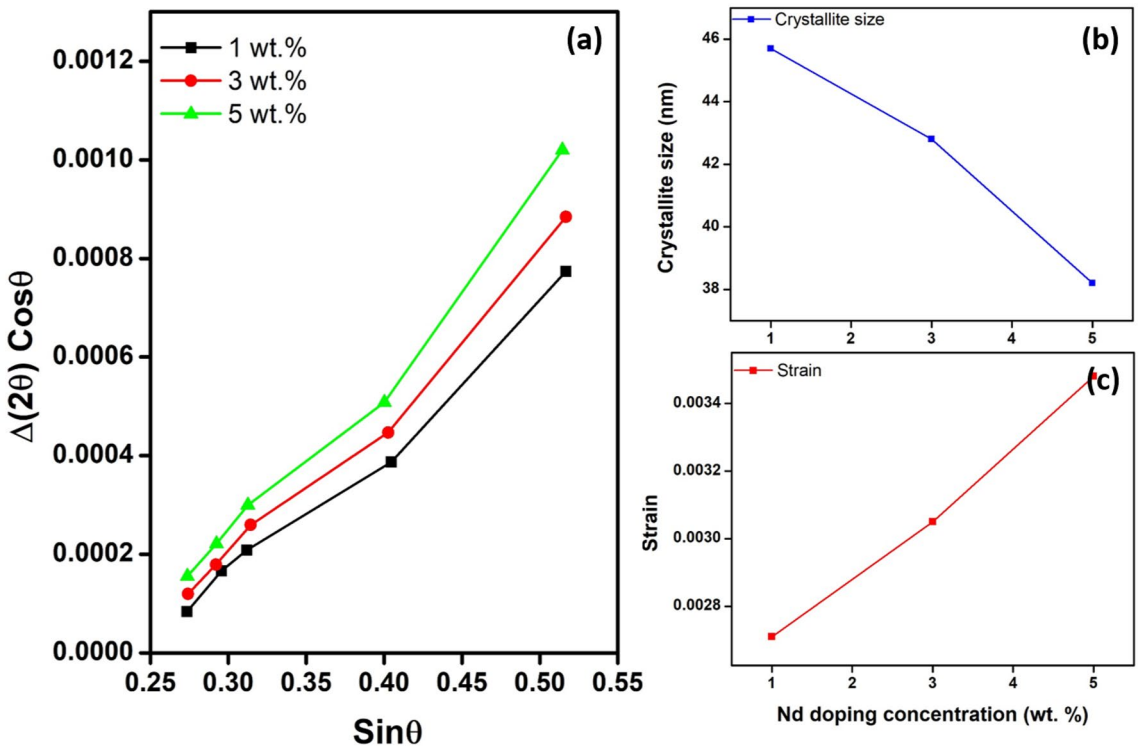


**Fig. 3** **a** Plot of Willamson–Hall equation of Δ(2θ) cos$\theta$ versus sin$\theta$ and their derived, **b** crystallite size and **c** micro strain values for NZO thin films

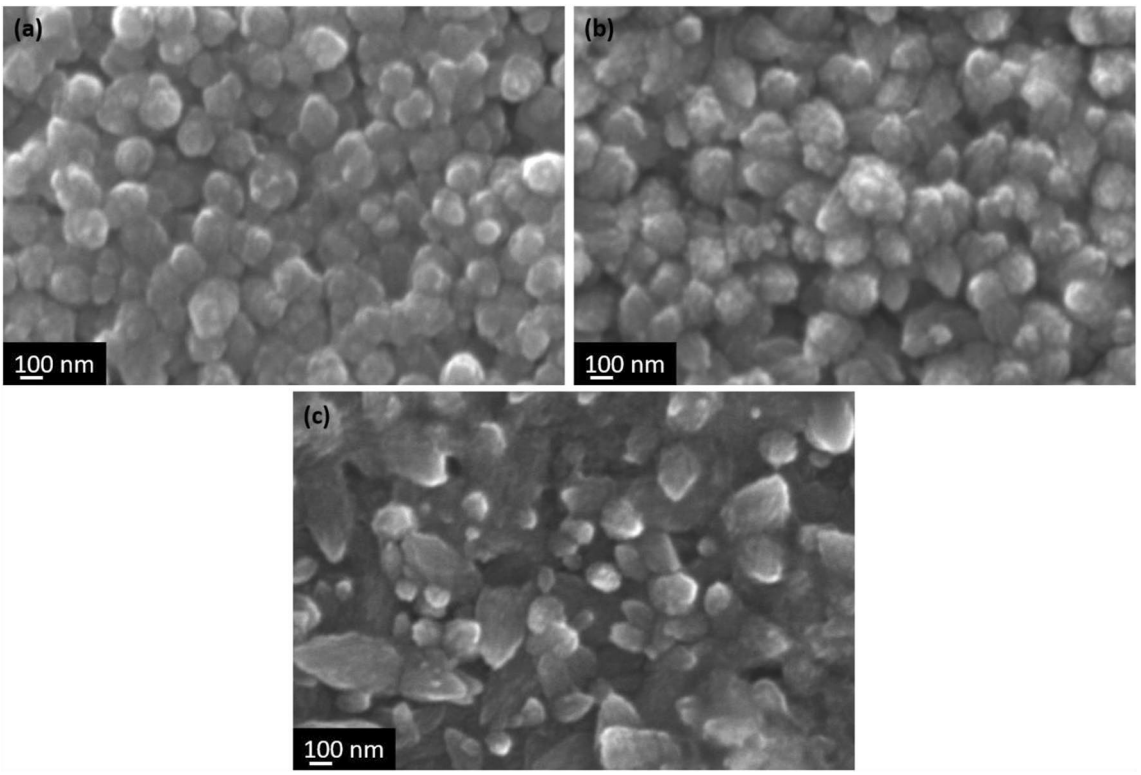


**Fig. 4** SEM micrographs of **a** 1, **b** 3 and **c** 5 wt% of Nd using prepared NZO thin films

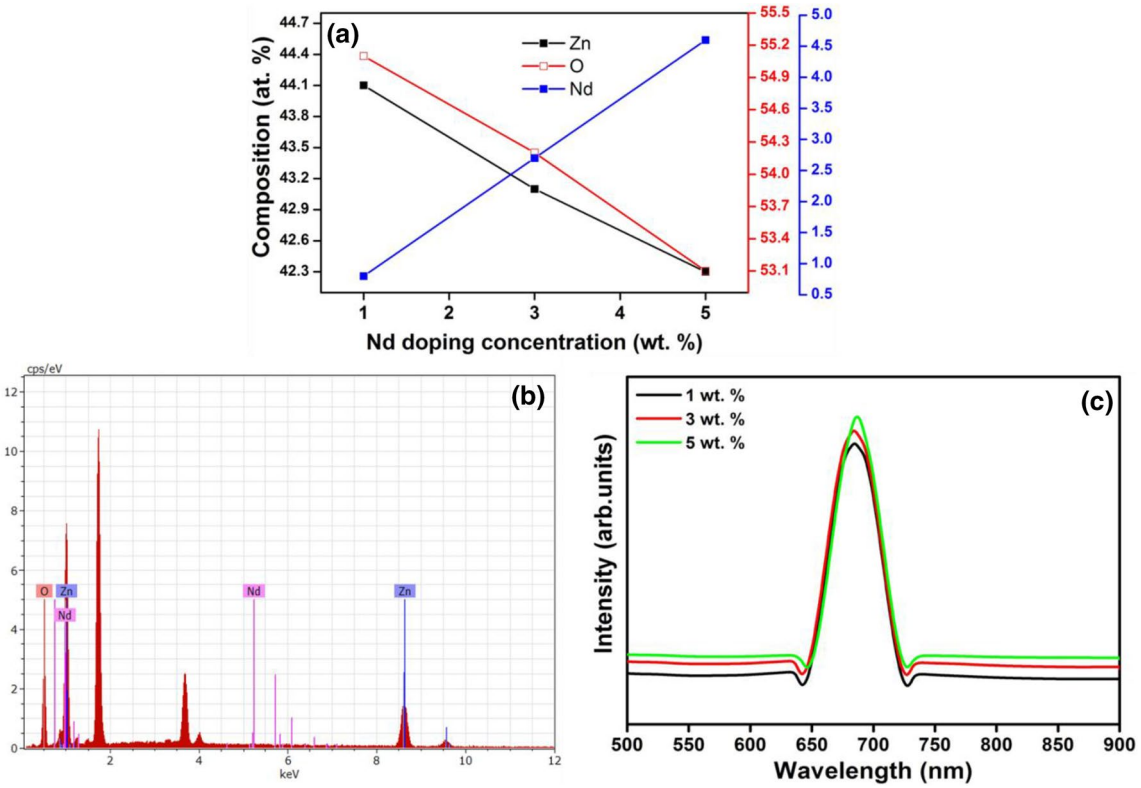


**Fig. 5** **a** Composition variations of NZO thin films with different wt% doped Nd; **b** EDAX spectrum of 5 wt% Nd doped NZO film; **c** photoluminescence spectra of NZO thin films with different wt% doped Nd

place of oxygen vacancies [34]. Recently, Rani et al. [35] have observed high intense PL peak around at ~680 nm. The emission peak intensity is also increased slightly when increase of Nd doping wt% for NZO thin films, which attributed to the surface defect.

Figure 6a displays the optical transmission profiles in the range of 350–1100 nm for different Nd doping wt% using prepared NZO thin films. The percentage of transmittance is differed from 90 to 80% for NZO thin films in the visible region and it is found to decline with increase of doping wt%, which is attributed to enhancement of thickness of film. All the NZO films are showing a sharp edge of absorption in the UV region around 375 nm due to the onset fundamental absorption. The observation of sharp absorption band for NZO film is inferred the good crystallinity with low defects, which is suitable for opto-electronic applications [36]. Also, transmittance can be reduced by increase of optical scattering which caused by the grain boundaries. NZO thin film, deposited using 1 wt% Nd, shows a high optical transmittance of about 90% in the visible region. This property can be defined by a less light scattering of NZO film (@1 wt%) due to its smooth surface and relatively a better crystallinity. The obvious grain boundary is exhibited for NZO (@1 wt% Nd) whereas 3 and 5 wt% Nd using prepared NZO films are not having obvious grains boundaries which evidently demonstrated by SEM (Fig. 4). The higher transmittance reveals the lesser defect density of NZO film because absorption of light in the longer wavelength region (>600 nm) affected by crystalline defects. Figure 6b shows the absorbance spectra of NZO films. NZO film is shown high percentage of absorbance in the UV region for 1 wt% Nd doping, whereas lower absorbance is observed in the visible region. The percentage of absorbance is gradually increased when the doping concentration is increased for NZO films.

Optical band gap by direct transition for NZO thin films were derived using the relation between incident photon energy (h$\nu$) and absorption coefficient ($\alpha$) as follow [37]

$$\alpha h\nu = B\left(h\nu - E_g\right)^n \tag{5}$$

where $E_g$ and B are optical band gap and constant, respectively. Figure 6c shows the Tauc's plots of different wt% using prepared NZO films and their band gap values were estimated by extrapolating to zero 'x' axis. Optical band gap value is lying between 3.17 and 3.22 eV [13]. The band gap reduction is directly related to the shift of absorption band edge and surface modification. The similar behavior of band gap decrement in terms of doping percentage is observed in the earlier reports for other metal dopant with ZnO [38, 39].

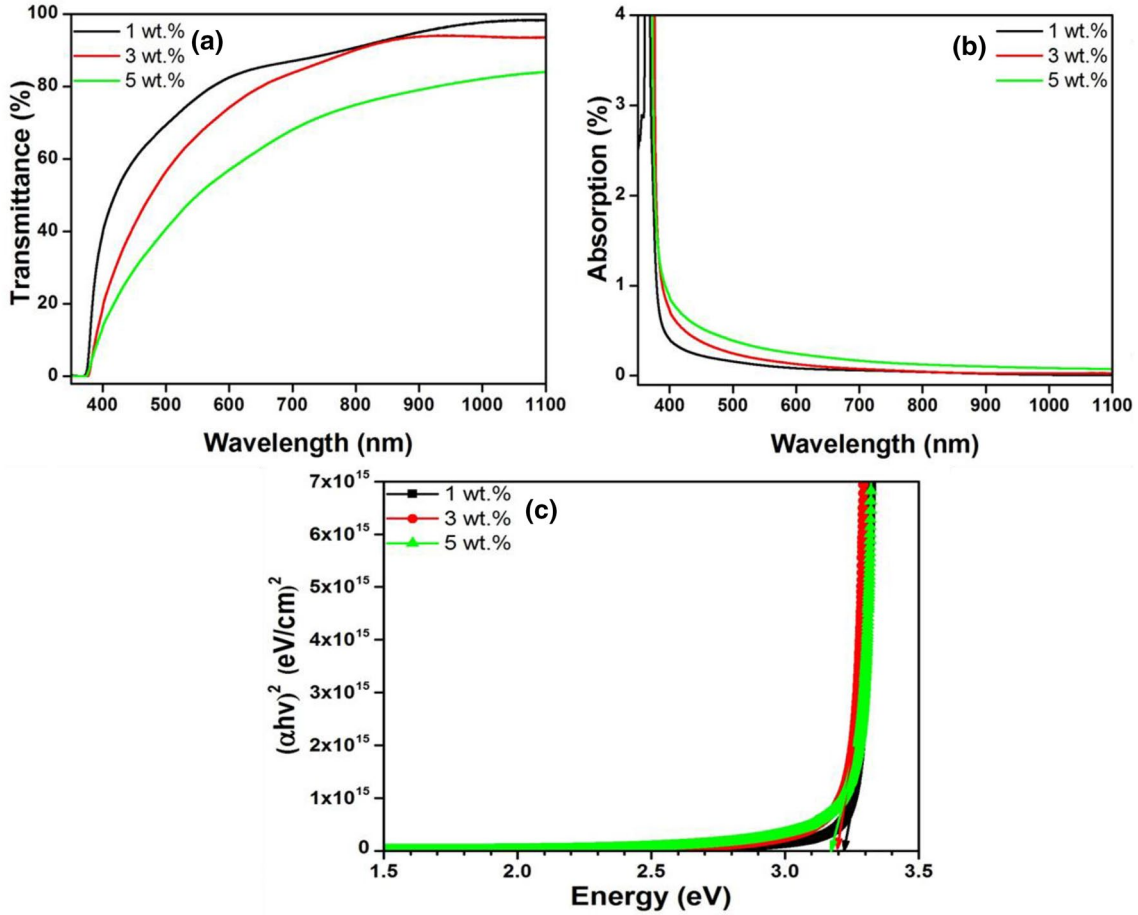


**Fig. 6** **a** Transmittance spectra, **b** absorption spectra and **c** Tauc's plots of NZO thin films

For optoelectronic devices, refractive indexes are major factor to determine their properties. Figure 7a shows the refractive index ($n$) variation in terms of wavelength for different Nd wt% using prepared NZO thin films. Refractive index were calculated using transmittance values by the revised algorithm of Swanepoel envelope method [40, 41]. From the Fig. 7a, refractive index values are deteriorated as a function of wavelength for NZO thin films. In addition, refractive index values are increased with increase of doping wt% for NZO which is due to increase of film thickness. Refractive index values are exhibited in the range between 2 and 4 for the visible range of wavelength for NZO. The extinction coefficient ($k$) of NZO thin films were determined by the reported procedure [30]. Figure 7b describes the alteration of extinction coefficient in terms of wavelength for NZO thin films. The extinction coefficient is increased as increase of Nd doping wt% for NZO thin films which attributed to enhance of absorption coefficient [41]. The observed results suggested that the NZO films are showed normal dispersions behavior in the UV–Vis–NIR region. The complex dielectric constant variations for different doping wt% using prepared NZO thin films are shown in Fig. 7c, d. The real and imaginary part of dielectric constant values are directly related to the energy states density of forbidden gap for the examined oxides [42]. The observed real and imaginary part of dielectric constant values are decreased against wavelength for all the NZO film due to the observed pattern of refractive index results. The complex dielectric constant values are increased with rise of doping wt% which is attributed to the increment of refractive indices. In addition, the observation of higher dielectric values are corresponded to the increase of atomic lattice imperfection [26].

Optical conductivity describes materials' photons transport and it is an influential tool to calibrate the electronic states of semiconductors [43]. The refractive index and absorption coefficient values were used to estimate the optical conductivity for different doping wt% using prepared NZO thin films as presented in the Fig. 8a. The optical conductivity is produced by the inter band transition which is initiated by phonon–electron interactions [43, 44]. The plasma frequency and static dielectric constant have been calculated from the plot of dielectric

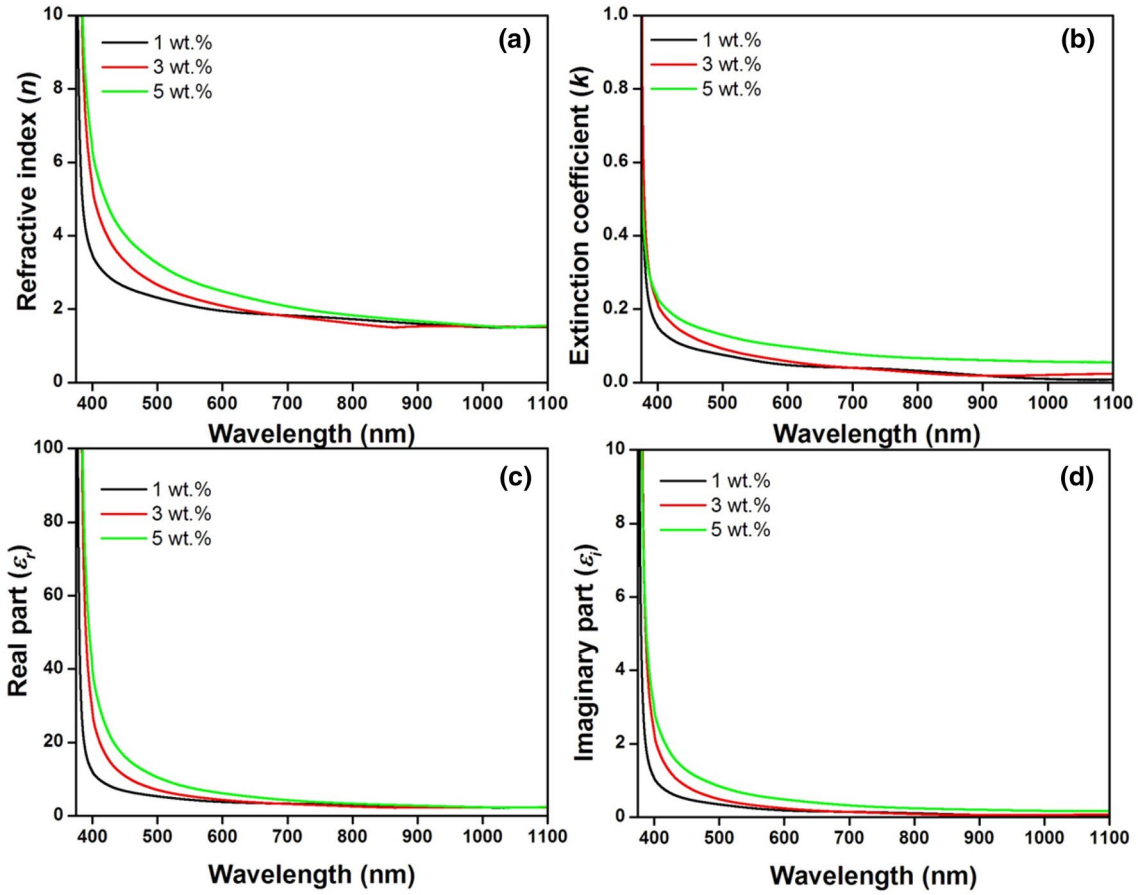


**Fig. 7** The variation of refractive indices **a** refractive index and **b** extinction coefficient; Dielectric constants for **c** real and **d** imaginary part as a function of wave length for NZO thin films

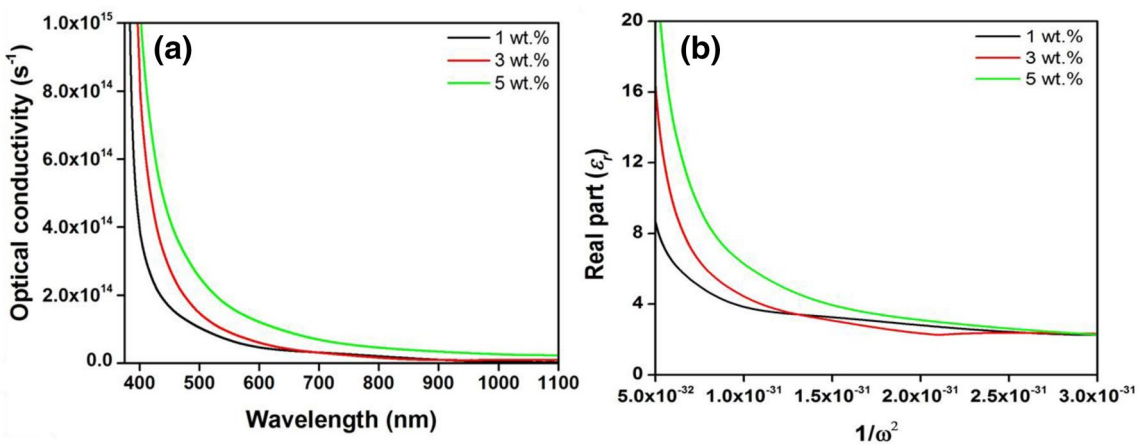


**Fig. 8** **a** Optical conductivity versus wavelength and **b** $\varepsilon_r$ versus $(1/\omega^2)$spectra for NZO thin films

constant versus $(1/\omega^2)$ shown in Fig. 8b which expressions are given in (6, 7) [26, 45]

$$\varepsilon_r = \varepsilon_\infty - (\varepsilon_\infty \omega_p^2)/\omega^2 \tag{6}$$

$$\varepsilon_r = \varepsilon_\infty - \left[e^2/\pi c^2\right](N/m^*)\lambda^2 \tag{7}$$

where $\varepsilon_\infty$ is static dielectric, c is velocity of light, e is charge of electron, N is carrier concentration, m* is mass and λ is wavelength. The estimated static dielectric constant, plasma frequency and carrier concentrations values are presented in Table 1 with respect to doping wt%. The static dielectric constant ($\varepsilon_\infty$) value is 7.1 for 1 wt% Nd using prepared NZO film, which is increased with increase of Nd wt% for NZO. The higher value of plasma frequency value is estimated at $1.88 \times 10^{15}$ $s^{-1}$ for NZO film prepared using 5 wt% Nd. The maximum value of carrier concentration is observed at $2.71 \times 10^{19}$ $cm^{-3}$ for NZO thin film prepared using 5 wt% Nd.

Hall measurements were performed in four-probe vander Pauw configuration at room temperature. The variation of electrical properties of NZO films as a function of different doping concentration is shown in Fig. 9a. These results suggest n-type semiconductor properties of NZO films due to the occurrence of interstitial oxygen vacancies and Zn atoms. The resistivity values are decreased with increase of doping concentration as shown in Fig. 9a. From the variation of carrier concentration, the incorporation of Nd ions are stimulated to provide more free electrons hence that carrier concentration is rapidly increased with Nd doping wt%. The observed electrical carrier concentration values are consistent with our optical approximation route estimated values. Moreover, carrier mobility is also increased with incorporation of Nd element in ZnO matrix. Accordingly, there are two reasons for enhancement of carrier concentration for NZO system; (i) substitution of $Nd^{3+}$ into $Zn^{2+}$ position and (ii) $Nd^{3+}$ is incorporated into the ZnO matrix. The possible mechanisms of high electrical properties for NZO matrix system is illustrated in Fig. 9b. The low value of electrical resistivity is observed at $3.82 \times 10^{-3}$ Ω cm for NZO thin film (@5 wt% Nd). The crystallinity of NZO thin film is highly influenced the transport properties [46]. This characteristic

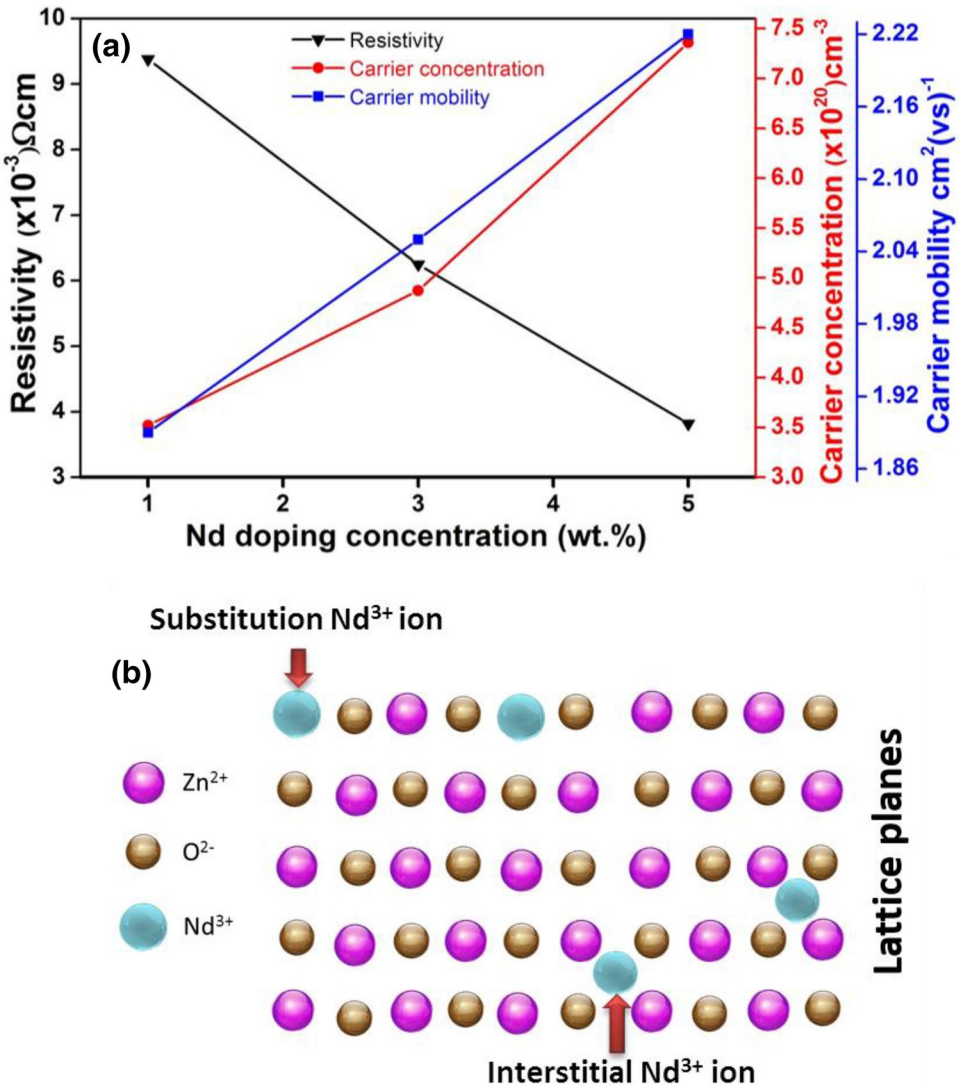


**Fig. 9** **a** The electrical resistively (ρ), carrier concentration (n) and carrier mobility (μ) of NZO thin films with respect to Nd doping concentrations; **b** possible mechanism for the incorporation of Nd into the ZnO lattice

nature can be lead to enrich the carrier concentration and mobility in terms of film thickness.

In general, TCO materials are needed to produce high transmittance values in the visible range and low electrical resistivity for better optoelectronic devices [47]. In our case, the obtained low resistivity and high optical transmittance for 5 wt% Nd doping are enabled to confirm the suitability of NZO thin film for optoelectronic device.

## 4 Conclusions

Thin films of NZO were efficaciously deposited by nebulized spray pyrolysis method using different Nd doping wt% on glass substrates. The electrical, optical and structural properties were elaborately discussed with doping concentration for NZO thin films. XRD patterns confirmed polycrystallinity of wurtzite structured NZO films. Different Nd doping wt% using prepared NZO thin films showed (002) preferential orientation. NZO film, coated using 1 wt% of Nd doping, has lower value of strain and higher value of crystallite size which compared to other Nd doping wt%. EDAX profile endorsed the existence of Zn, O and Nd in the NZO film. Band gap values were found to be 3.21 eV to 3.17 eV for different Nd doping wt% using prepared NZO films. Optical parameters of dielectric constants ($\varepsilon$), refractive indices ($n$ & $k$), carrier concentration (N) and plasma frequency ($\omega_p$) were evaluated for NZO through optical approximation route. The carrier concentration and Hall mobility values were found to be increased with increase of Nd doping wt%. From the observed optical and electrical results of NZO thin films, it would be suitable candidate for various opto-electronic applications.

**Acknowledgements** The authors extend their appreciation to the Deanship of Scientific Research at King Khalid University for funding this work through General Research Project under grant number (R.G.P.1/45/39). Also, this work was partly supported by the Ministry of Trade, Industry and Energy (MOTIE, Korea) under Sensor Industrial Technology Innovation Program (No. 10063682), and the Basic Science Research Program through the National Research Foundation of Korea (NRF) funded by the Ministry of Education (2017R1D1A1A09000823).

## References

1. Z.L. Wang, J. Song, Piezoelectric nanogenerators based on zinc oxide nanowire arrays. Science **312**(5771), 242–246 (2006)
2. M. Subramanian, P. Thakur, S. Gautam, K. Chae, M. Tanemura, T. Hihara, S. Vijayalakshmi, T. Soga, S. Kim, K. Asokan, Investigations on the structural, optical and electronic properties of Nd doped ZnO thin films. J. Phys. D Appl. Phys. **42**(10), 105410 (2009)
3. C. Cheng, R. Xin, Y. Leng, D. Yu, N. Wang, Chemical stability of ZnO nanostructures in simulated physiological environments and its application in determining polar directions. Inorg. Chem. **47**(17), 7868–7873 (2008)
4. H. Serier, M. Gaudon, M. Ménétrier, Al-doped ZnO powdered materials: Al solubility limit and IR absorption properties. Solid State Sci. **11**(7), 1192–1197 (2009)
5. V. Gokulakrishnan, S. Parthiban, K. Jeganathan, K. Ramamurthi, Investigation on the effect of Zr doping in ZnO thin films by spray pyrolysis. Appl. Surf. Sci. **257**(21), 9068–9072 (2011)
6. S. Thiagarajan, A. Sanmugam, D. Vikraman, in Facile methodology of sol-gel synthesis for metal oxide nanostructures, ed. by Chandra U. *Recent Applications in Sol-Gel Synthesis* (InTech, Rijeka, 2017) pp 1–16
7. V. Bhavanasi, C.B. Singh, D. Datta, V. Singh, K. Shahi, S. Kumar, Structural, optical and light scattering properties of post etched RF sputtered ZnO: Al thin films deposited at various substrate temperature. Opt. Mater. **35**(7), 1352–1359 (2013)
8. A. Ghosh, N. Deshpande, Y. Gudage, R. Joshi, A. Sagade, D. Phase, R. Sharma, Effect of annealing on structural and optical properties of zinc oxide thin film deposited by successive ionic layer adsorption and reaction technique. J. Alloys Compd. **469**(1), 56–60 (2009)
9. K. Shamala, L. Murthy, K.N. Rao, Studies on tin oxide films prepared by electron beam evaporation and spray pyrolysis methods. Bull. Mater. Sci. **27**(3), 295–301 (2004)
10. R. Ding, C. Xu, B. Gu, Z. Shi, H. Wang, L. Ba, Z. Xiao, Effects of Mg incorporation on microstructure and optical properties of ZnO thin films prepared by sol-gel method. J. Mater. Sci. Technol. **26**(7), 601–604 (2010)
11. P. Ravikumar, K. Ravichandran, B. Sakthivel, Effect of thickness of $SnO_2$:F over layer on certain physical properties of ZnO:Al thin films for opto-electronic applications. J. Mater. Sci. Technol. **28**(11), 999–1003 (2012)
12. Z. Zhi, Y. Liu, B. Li, X. Zhang, Y. Lu, D. Shen, X. Fan, Effects of thermal annealing on ZnO films grown by plasma enhanced chemical vapour deposition from Zn $(C_2H_5)_2$ and $CO_2$ gas mixtures. J. Phys. D Appl. Phys. **36**(6), 719 (2003)
13. R. Chandramohan, T. Vijayan, S. Arumugam, H. Ramalingam, V. Dhanasekaran, K. Sundaram, T. Mahalingam, Effect of heat treatment on microstructural and optical properties of CBD grown Al-doped ZnO thin films. Mater. Sci. Eng. B **176**(2), 152–156 (2011)
14. X. Liang, Y. Ren, S. Bai, N. Zhang, X. Dai, X. Wang, H. He, C. Jin, Z. Ye, Q. Chen, L. Chen, J. Wang, Y. Jin, Colloidal indium-doped zinc oxide nanocrystals with tunable work function: rational synthesis and optoelectronic applications. Chem. Mater. **26**(17), 5169–5178 (2014). https://doi.org/10.1021/cm502812c
15. J.H. Hsieh, C.K. Chang, H.H. Hsieh, Y.J. Cho, J. Lin, Electrical and optical properties of gallium-doped zinc oxide thin films prepared by Ion-Beam-Assisted Deposition. Vacuum **118**, 43–47 (2015)
16. X.-H. Zhang, J. Chen, Y. Wu, Z. Xie, J. Kang, L. Zheng, A simple route to fabricate high sensibility gas sensors based on erbium doped ZnO nanocrystals. Colloids Surf. A **384**(1), 580–584 (2011)
17. W.E. Mahmoud, Synthesis and optical properties of Ce-doped ZnO hexagonal nanoplatelets. J. Cryst. Growth **312**(21), 3075–3079 (2010)
18. X. Zhang, W. Mi, X. Wang, H. Bai, First-principles prediction of electronic structure and magnetic ordering of rare-earth metals doped ZnO. J. Alloys Compd. **617**, 828–833 (2014)
19. A. El Hachimi, H. Zaari, A. Benyoussef, M. El Yadari, A. El Kenz, First-principles prediction of the magnetism of 4f rare-earth-metal-doped wurtzite zinc oxide. J. Rare Earth **32**(8), 715–721 (2014)

20. A. Douayar, M. Abd-Lefdil, K. Nouneh, P. Prieto, R. Diaz, A. Fedorchuk, I. Kityk, Photoinduced Pockels effect in the Nd-doped ZnO oriented nanofilms. Appl. Phys. B **110**(3), 419–423 (2013)
21. Y. Liu, W. Luo, R. Li, X. Chen, Optical properties of $Nd^{3+}$ ion-doped ZnO nanocrystals. J. Nanosci. Nanotechnol. **10**(3), 1871–1876 (2010)
22. A. Douayar, P. Prieto, G. Schmerber, K. Nouneh, R. Diaz, I. Chaki, S. Colis, A. El Fakir, N. Hassanain, A. Belayachi, Investigation of the structural, optical and electrical properties of Nd-doped ZnO thin films deposited by spray pyrolysis. Eur. Phys. J. Appl. Phys. **61**(1), 10304 (2013)
23. F. Xian, X. Li, Effect of Nd doping level on optical and structural properties of ZnO: Nd thin films synthesized by the sol–gel route. Opt. Laser Technol. **45**, 508–512 (2013)
24. M. Nistor, E. Millon, C. Cachoncinlle, W. Seiler, N. Jedrecy, C. Hebert, J. Perrière, Transparent conductive Nd-doped ZnO thin films. J. Phys. D Appl. Phys. **48**(19), 195103 (2015)
25. M. Nistor, L. Mihut, E. Millon, C. Cachoncinlle, C. Hebert, J. Perriere, Tailored electric and optical properties of Nd doped ZnO: from transparent conducting oxide to photon down-shifting thin films. RSC Adv. **6**(47), 41465–41472 (2016)
26. D. Vikraman, H.J. Park, S.-I. Kim, M. Thaiyan, Magnetic, structural and optical behavior of cupric oxide layers for solar cells. J. Alloys Compd. **686**, 616–627 (2016)
27. J. Zheng, J. Song, Z. Zhao, Q. Jiang, J. Lian, Optical and magnetic properties of Nd-doped ZnO nanoparticles. Cryst. Res. Tech. **47**(7), 713–718 (2012)
28. T.A. Vijayan, R. Chandramohan, S. Valanarasu, J. Thirumalai, S. Venkateswaran, T. Mahalingam, S.R. Srikumar, Optimization of growth conditions of ZnO nano thin films by chemical double dip technique. Sci. Tech. Adv. Mater. **9**(3), 035007 (2008)
29. T. Mahalingam, V. Dhanasekaran, G. Ravi, S. Lee, J. Chu, H.-J. LIW, Effect of deposition potential on the physical properties of electrodeposited CuO thin films. J. Optoelectron Adv. M **12**(6), 1327–1332 (2010)
30. V. Dhanasekaran, T. Mahalingam, Physical properties evaluation of various substrates coated cupric oxide thin films by dip method. J. Alloys Compd. **539**, 50–56 (2012)
31. R. Kasar, N. Deshpande, Y. Gudage, J. Vyas, R. Sharma, Studies and correlation among the structural, optical and electrical parameters of spray-deposited tin oxide ($SnO_2$) thin films with different substrate temperatures. Phys. B Condens. Matter **403**(19), 3724–3729 (2008)
32. T. Mahalingam, V. Dhanasekaran, R. Chandramohan, J.-K. Rhee, Microstructural properties of electrochemically synthesized ZnSe thin films. J. Mater. Sci. **47**(4), 1950–1957 (2012). https://doi.org/10.1007/s10853-011-5989-3
33. W. Dong, C. Zhu, Optical properties of surface-modified CdO nanoparticles. Opt. Mater. **22**(3), 227–233 (2003)
34. T. Subramanyam, B. Srinivasulu Naidu, S. Uthanna, Structure and optical properties of dc reactive magnetron sputtered zinc oxide films. Cryst. Res. Tech. **34**(8), 981–988 (1999)
35. T.D. Rani, K. Tamilarasan, K. Thangaraj, E. Elamurugu, K. Ramamurthi, S. Leela, Structural and optical properties of $Nd^{3+}$ doped zinc oxide thin films deposited by spray pyrolysis. Optik **127**(1), 72–75 (2016)
36. K. Ravichandran, R. Mohan, N.J. Begum, S. Snega, K. Swaminathan, C. Ravidhas, B. Sakthivel, S. Varadharajaperumal, Impact of spray flux density and vacuum annealing on the transparent conducting properties of doubly doped (Sn + F) zinc oxide films deposited using a simplified spray technique. Vacuum **107**, 68–76 (2014)
37. J. Tauc, *Amorphous and Liquid Semiconductors*. (Springer Science & Business Media, Berlin, 2012)
38. Y. Hu, Y. Chen, Z. Zhong, C. Yu, G. Chen, P. Huang, W.-Y. Chou, J. Chang, C. Wang, The morphology and optical properties of Cr-doped ZnO films grown using the magnetron co-sputtering method. Appl. Surf. Sci. **254**(13), 3873–3878 (2008)
39. L. Li, W. Wang, H. Liu, X. Liu, Q. Song, S. Ren, First principles calculations of electronic band structure and optical properties of Cr-doped ZnO. J. Phys. Chem. C **113**(19), 8460–8464 (2009)
40. R. Swanepoel, Determination of the thickness and optical constants of amorphous silicon. J. Phys. E Sci. Instrum. **16**(12), 1214 (1983)
41. V. Dhanasekaran, T. Mahalingam, J.-K. Rhee, J. Chu, Structural and optical properties of electrosynthesized ZnSe thin films. Opt. Int. J. Light Electron Opt. **124**(3), 255–260 (2013)
42. E. Márquez, A.M. Bernal-Oliva, J.M. González-Leal, R. Prieto-Alcón, A. Ledesma, R. Jiménez-Garay, I. Mártil, Optical-constant calculation of non-uniform thickness thin films of the Ge10As15Se75 chalcogenide glassy alloy in the sub-band-gap region (0.1–1.8 eV). Mater. Chem. Phys. **60**(3), 231–239 (1999)
43. S. Thiagarajan, M. Thaiyan, R. Ganesan, Physical property exploration of highly oriented $V_2O_5$ thin films prepared by electron beam evaporation. New J. Chem. **39**(12), 9471–9479 (2015). https://doi.org/10.1039/C5NJ01582K
44. P.B. Johnson, R.W. Christy, Optical constants of transition metals: Ti, V, Cr, Mn, Fe, Co, Ni, and Pd. Phys. Rev. B **9**(12), 5056–5070 (1974)
45. Res IAE, Res. J. Recent Sci. **1**, 46 (2012)
46. J.W. Orton, M.J. Powell, The Hall effect in polycrystalline and powdered semiconductors. Rep. Prog. Phys. **43**(11), 1263 (1980)
47. V. Anand, A. Sakthivelu, K.D.A. Kumar, S. Valanarasu, V. Ganesh, M. Shkir, S. AlFaify, H. Algarni, Rare earth $Eu^{3+}$ co-doped AZO thin films prepared by nebulizer spray pyrolysis technique for optoelectronics. J. Sol-Gel. Sci. Technol. **86**(2), 293–304 (2018)